Arabian Journal of Chemistry (2016) xxx, xxx–xxx

King Saud University

Arabian Journal of Chemistry

www.ksu.edu.sa
www.sciencedirect.com

ORIGINAL ARTICLE

Synthesis of functionalized Cu:ZnS nanosystems and its antibacterial potential

C. Chaliha [a], B.K. Nath [a], P.K. Verma [b], E. Kalita [a,*]

[a] Department of Molecular Biology and Biotechnology, Tezpur University, Tezpur, Assam 784028, India
[b] National Institute of Plant Genome Research, Aruna Asaf Ali Marg, P.O. Box No. 10531, New Delhi 110 067, India

Received 5 February 2016; accepted 7 May 2016

KEYWORDS

Cu:ZnS;
MSA;
Sodium citrate;
Solvothermal;
ζ potential;
Antibacterial property

Abstract Copper doped Zinc Sulfide (Cu:ZnS) nanoparticles were synthesized as potential antibacterial agents, through a solvothermal approach using Mercaptosuccinic acid (MSA) and Sodium citrate (SC) as differential capping agents. Multiple variants of the Cu:ZnS nanoparticles were generated based on the refluxing intervals of the reactions and a choice of the capping agents. The microstructural properties and the elemental composition of the synthesized nanosystems were examined using Scanning Electron Microscopy (SEM) and powder X-ray Diffraction (XRD), along with Energy-Dispersive X-ray spectroscopy (EDX) and Microwave Plasma-Atomic Emission Spectroscopy (MP-AES). The as-synthesized nanosystems were also characterized for their surface attributes using Fourier Transform Infrared spectroscopy (FT-IR), while the optical properties were studied using UV–Vis spectroscopy. The electrostatic stability of the aqueous dispersions of Cu:ZnS was studied as a function of their solvent pH, using Photon Correlation Spectroscopy. For the assessment of the antibacterial properties of the different variants of Cu:ZnS nanosystems, the disk diffusion assay was performed against both Gram-positive and Gram-negative bacteria. The results show a promising antibacterial activity for the Cu:ZnS variants synthesized, with a prominent activity in the MSA@Cu:ZnS nanoparticle making them a novel class of potential antibacterial agents.

1. Introduction

The exploration of nanoparticles for antimicrobial applications is gaining increasing significance due to the emergence of microbial resistance against the conventional drug regime (Pelgrift and Friedman, 2013; Dhivya et al., 2015). Silver (Ag), Gold (Au) and Titanium (Ti) nanoparticles, that harbor antibacterial properties have been widely employed in health care and food industries as bactericidal or bacteriostatic agents, thereby curtailing the use of antibiotics/antibacterials in general (Bokare et al., 2013; Tam et al., 2008). In the present context, the advent of facile and economical synthesis routes for other nanoparticles such as Copper (Cu), Zinc Oxide (ZnO), and Zinc Sulfide (ZnS)

* Corresponding author. Tel.: +91 3712 275411.
E-mail addresses: ekalita@tezu.ernet.in, eeshankalita@gmail.com (E. Kalita).
Peer review under responsibility of King Saud University.

Production and hosting by Elsevier

http://dx.doi.org/10.1016/j.arabjc.2016.05.002

showing similar antimicrobial potential, has resulted in their exploration as viable alternatives (Ruparelia et al., 2008; Talebian et al., 2013; Suyana et al., 2014). Of these, Zinc Sulfide (ZnS) nanoparticles are noteworthy II-IV group semiconductors with a wide band gap energy (3.68 eV) which are conventionally used as biosensors, fluorescent probes, UV-light and chemical sensors owing to their unusual luminescence properties (Fang et al., 2011). The tunability of the band gap energy for these materials has been achieved by an assortment of techniques including the introduction of trace amounts of transition metals such as Ni, Cu, Mn, and Co which has resulted in the enhancement of luminescence properties across a wider spectral range while also rendering novel attributes, due to the presence of the dopants (Murugadoss, 2012). With regard to the antimicrobial activity, preliminary reports on Mn doped ZnS nanosystems have shown some promise as antibacterials (Singh et al., 2014). However Cu:ZnS nanosystems have been so far investigated more in relation to their electro-optical properties rather than as antibacterials, despite the Zn and Cu based nanoparticles being established as prominent antibacterials. This provides an elementary framework for the exploration of Cu:ZnS nanosystems as potential antibacterials. It has been reported however, that the native ZnS readily undergoes oxidation to ZnO under atmospheric conditions, which significantly compromises its stability and efficacy (Namsani et al., 2015). Reports exist on the use of various capping agents *viz*. gelatin, citric acid, biotin, polyethylene glycol (PEG), and pepsin in an effort to retain the activity of such nanoparticles, which also helps in achieving better control over their size and tunability (Mohan et al., 2014; Singh et al., 2014). Hence, the current study aspires to achieve a balanced antibacterial activity in the Cu:ZnS nanosystems, using Cu as the dopant along with a suitable capping agent.

In the present study Cu:ZnS nanosystems were synthesized using a solvothermal approach with two differential capping agents *viz*. Mercaptosuccinic (MSA) acid and Sodium citrate (SC) for the synthesis of a potential antibacterial system. The as prepared nanosystems were characterized using powder X-ray Diffraction (XRD) spectroscopy, Fourier Transform Infrared spectroscopy (FTIR) and UV-PL spectroscopy. The average size of the nanosystems was estimated using Scanning Electron Microscopy (SEM) and Photon Correlation Spectroscopy and the electrostatic stability of the nanosystems was assessed via surface charge (ζ potential) analysis. Furthermore, the synthesized nanosystems were quantitatively assessed for their antibacterial properties against both Gram-positive *Bacillus subtilis* (ATCC 11774) and Gram-negative *Escherichia coli* (NCTC 10538) using disk diffusion assay.

2. Materials and methods

2.1. Chemicals

Zinc chloride ($ZnCl_2$), copper acetate ($Cu(CH_3COO)_2$), sodium sulphide (Na_2SO_3) and sodium borohydride ($NaBH_4$) of analytical grade were purchased from Sigma–Aldrich, India. Mercaptosuccinic acid ($C_4H_6O_4S$), and Sodium citrate ($NaC_6H_5O_7$) were purchased from Sigma–Aldrich, India, and were used as capping agents.

2.2. Synthesis of Cu doped ZnS nanoparticles

Cu:ZnS nanoparticles were synthesized using a modified solvothermal approach (Wu et al., 2012). Stoichiometric amounts of $ZnCl_2$ (8 mM), Na_2SO_3 (50 mM) and $Cu(CH_3COO)_2$ (2 mM) were used to obtain the solvothermal premix. Each of the capping agents, *viz*. Sodium citrate (19 mM) and Mercaptosuccinic acid (19 mM) was then added separately into the premix, in separate reaction setups (Fig. 1).

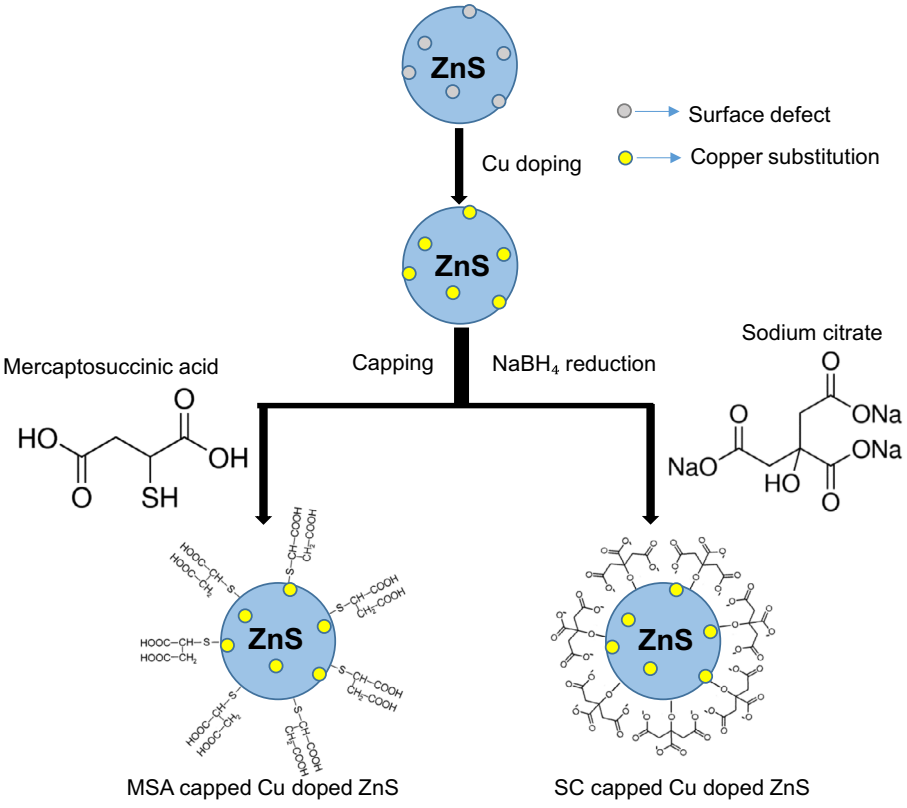

Figure 1 Schematic representation of the synthesis of MSA@Cu:ZnS and SC@Cu:ZnS nanosystems.

The as prepared reaction mixture was then stirred on a magnetic stirrer for a period of 1 h with gradual addition of $NaBH_4$ (75 mM) to function as a reducing agent. It was then transferred into a round bottom flask and was subjected to solvothermal treatment at a temperature of ~100 °C for different reflux intervals *viz*. 1–5 h to generate the time based variants. The solvothermal extract was cooled to room temperature, followed by washing with copious amounts of de-ionised water and ethanol to remove all unreacted precursors. The washed nanosystems were finally oven dried at a temperature of 60 °C for a period of 48 h.

2.3. Characterization of synthesized nanosystems

The Scanning Electron Microscopy (SEM) studies for the synthesized nanosystems were performed using a JSM-6390, JEOL, scanning electron microscope (Singapore). The samples were mounted onto carbon grids and analysed for elemental composition using SEM equipped with Energy Dispersive X-ray Diffraction spectroscopy (EDX). The Elemental map for both the nanosystems was generated using pseudo-colours to characterize the distribution of the elements present in the synthesized nanosystems. The EDX data were further validated by quantitative estimation of Zn and Cu using a MP-AES 4200 Microwave Plasma – Atomic Emission Spectrophotometer (Agilent Technologies). The X-ray diffractograms were obtained with the help of a Miniflex tabletop X-ray diffractometer from Rigaku corporation, Japan, using monochromatic Cu kα radiation (λ = 1.54 Å). The operating voltage and current were set at 40 kV and 15 mA respectively to generate the diffractograms of the samples. To obtain the Fourier Transform Infrared (FTIR) spectra, the synthesized nanosystems were ground with Potassium Bromide (KBr) and subsequently pelletized using a Qwik-Handi Press Kit (Perkin Elmer USA). The FTIR spectra of the translucent pellet were recorded using a Perkin Elmer LS55 Fourier transform infrared spectrometer (USA) in the range of 500–4000 cm^{-1}. Additionally, the absorption spectra of the synthesized nanosystems were obtained in the range of 200–800 nm using a Thermo Scientific UV-10 UV–Vis spectrophotometer. The photoluminescence (PL) excitation spectra of the samples were also recorded using a Perkin Elmer LS55 fluorescence spectrophotometer.

2.4. Effect of pH on the size and the electrostatic stability of the synthesized nanosystems

The variation in the size of the dispersed nanosystems with respect to the change in solvent pH was assessed by monitoring the change in their hydrodynamic diameter over different time periods of incubation. The samples were diluted to 100× using deionised water and sonicated for 10 min (Sartorius labsonic M, Germany) at a frequency of 24 kHz. The variation in the size of the nanosystems was investigated using a Zetasizer Nano-ZS-90 Dynamic Light Scattering system (Malvern Instruments, UK) operating at a wavelength of 633 nm and a scattering angle of 90°, under a constant temperature of 25 °C.

Aqueous dispersions of the nanosystems were assessed for their electrostatic stability by analyzing their surface charge (ζ potential) with respect to the change in solvent pH over different time periods of incubation. The surface charge was measured using a Zetasizer Nano-ZS-90 (Malvern Instruments, UK) based on the electrophoretic mobility of the dispersed nanosystems. Further, the functionalized nanosystems were incubated in de-ionized water for a period of 48 h and the concentration of Zn and Cu leachate from both the nanosystems was estimated using Microwave Plasma-Atomic Emission spectroscopy (MP-AES).

2.5. Antibacterial assay

The synthesized nanosystems were tested for antibacterial properties against Gram-negative *Escherichia coli* (NCTC 10538) and Gram-positive *Bacillus subtilis* (ATCC 11774) by performing disk diffusion assay. The bacterial strains were inoculated in Luria–Bertani (LB) broth and were incubated overnight at 37 °C at 180 rpm in a shaking incubator. The inoculated bacterial cultures were then spread on LB agar plates. Sterile filter paper disks containing different concentrations of the synthesized nanosystems were then placed in the LB agar plates and were incubated overnight at temperature of 37 °C. Following incubation, the incubated plates were examined for the presence of a prominent zone of inhibition.

3. Results and discussion

3.1. Microstructural characterization

The SEM micrographs portraying the surface morphology for the 1 h time variant of the synthesized nanosystems are shown in Fig. 2a and b. The synthesized MSA@Cu:ZnS and SC@Cu:ZnS nanosystems are seen to exhibit a quasi-spherical morphology. Fig. 2c and d represents the particle size distribution for the Cu:ZnS nanosystems wherein the MSA@Cu:ZnS nanosystems have a narrower size distribution compared to the SC@Cu:ZnS nanosystems. Further, the average size of the MSA and SC functionalized Cu:ZnS nanosystems was estimated to be ~63 nm and ~85 nm respectively. The EDX spectra (Fig. 2a inset, b inset) confirmed the existence of Zn, S, Cu and O as elemental constituents in both the functionalized nanosystems with an estimated weight percentage of 45.66% and 18.01%, of Zn and 9.23% and 31.76% of Cu in the MSA@Cu:ZnS and SC@Cu:ZnS nanosystems, respectively (Table S1). The pseudo-colour elemental maps (Fig. 2e–l) for Zn, S, Cu and O of the MSA@Cu:ZnS and SC@Cu:ZnS nanosystems show a homogenous distribution of the elements throughout the area being investigated.

However, EDX being generally regarded as a semi-quantitative estimation for the elemental composition (Gao et al., 2015), the nanosystems were further subjected to Microwave Plasma-Atomic Emission Spectroscopy (MP-AES) based analysis. The molar ratio of Zn:Cu, derived from the AES experiments, was found to be ~3:1 for MSA@Cu:ZnS, while that of the SC@Cu:ZnS nanosystems was ~1:3 (Table S2). The results suggest a better degree of control during the synthesis of the MSA@Cu:ZnS, to derive a Copper doped ZnS system and is also in close agreement with the Zn:Cu precursor feed ratio of 4:1.

Fig. 3a and b shows the X-ray diffractogram of the MSA@Cu:ZnS and SC@Cu:ZnS nanoparticles. Both the diffractograms show the presence of characteristic peaks for the zinc blende phase structure of ZnS at 2θ = 28.9°, 48.1°,

Please cite this article in press as: Chaliha, C. et al., Synthesis of functionalized Cu:ZnS nanosystems and its antibacterial potential. Arabian Journal of Chemistry (2016), http://dx.doi.org/10.1016/j.arabjc.2016.05.002

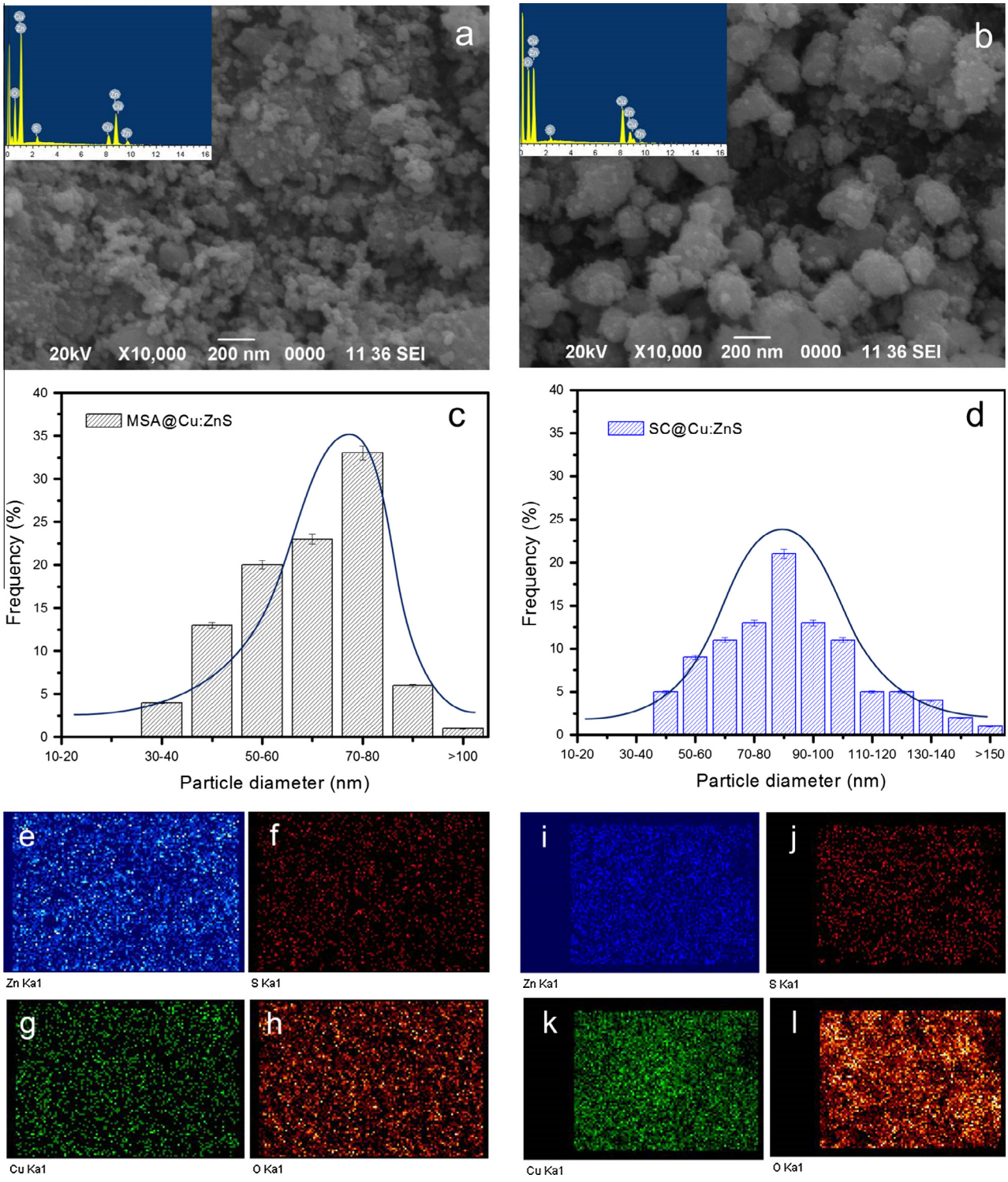

Figure 2 SEM micrographs of MSA@Cu:ZnS (a) and SC@Cu:ZnS (b), EDX of MSA@Cu:ZnS (a inset) and SC@Cu:ZnS (b inset), comparative particle size distribution of MSA@Cu:ZnS (c) and SC@Cu:ZnS (d) and pseudo-colour elemental distribution maps of MSA@Cu:ZnS (e–h), SC@Cu:ZnS (i–l).

and 57.1°, corresponding to the diffraction planes 111, 220 and 311 respectively (Chauhan et al., 2014). The radius of ionic Cu (0.057 nm) has been reported to be congruent to that of Zn (0.06 nm) and hence no separate crystallinity peak for Cu was observed in the diffractograms of the synthesized nanosystems (Lee et al., 2014). Furthermore, the shift in the peak position observed at $2\theta = 28.9°$ and 48.1° corresponding to the diffraction plane 111 and 220 respectively, validates the presence of Cu in the ZnS nanostructure, for both the systems (Bhuyan et al., 2015).

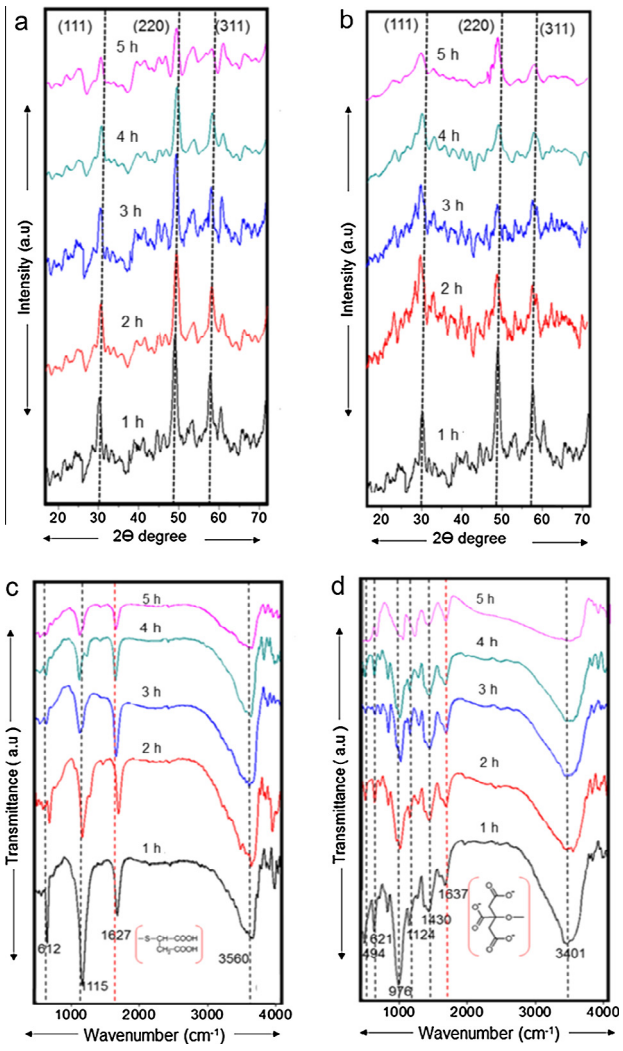

Figure 3 Comparative X-ray diffraction micrograph of MSA@Cu:ZnS (a), SC@Cu:ZnS (b) and FTIR spectra of MSA@Cu:ZnS (c), SC@Cu:ZnS (d) nanosystems of 1–5 h variants.

Fig. 3c and d shows the Fourier transform infrared (FTIR) spectra of the MSA@Cu:ZnS and SC@Cu:ZnS nanoparticles in the range of 500–4000 cm^{-1}. The FTIR spectra of MSA@Cu:ZnS nanosystems show the presence of characteristic Zn-S vibration peaks at 612 cm^{-1} and 1115 cm^{-1} (Kuppayee et al., 2011) along with an additional peak at 1627 cm^{-1} that corresponds to the stretching vibration of thiol group, which is indicative of an effective capping with MSA (Reghuram et al., 2015). The FTIR spectra of SC@Cu:ZnS nanosystems also show prominent Zn–S vibration peaks at 494 cm^{-1} and 621 cm^{-1} (Kuppayee et al., 2011) along with peaks at 976 cm^{-1} and 1124 cm^{-1} representative of the resonance interaction between Zn and Cu, thus indicating the incorporation of Cu as Cu–S–Zn in the nanosystems (Lee et al., 2014). The peak at 1637 cm^{-1} represents the symmetric carboxyl group of Sodium citrate thus suggesting the capping of the nanosystems by Sodium citrate (Cheng et al., 2009). The peaks in the range of 1430 cm^{-1} and the additional peaks observed between 3000 cm^{-1} and 3600 cm^{-1} may be attributed to C—O stretching vibration (Lee et al., 2014) and hydrogen stretching frequencies respectively (Agorku et al., 2015).

The doping of ZnS nanosystems using Cu was further validated from the UV–vis absorbance and PL emission studies of the synthesized nanosystems. The UV–vis absorbance spectra (Fig. 4a and g), show a hypsochromic shift in the transition peaks across the wavelength range of ~270–285 nm, with the increase in the period of synthesis for both the MSA@Cu:ZnS and SC@Cu:ZnS nanosystems. This hypsochromic shift observed for both the nanosystems, is indicative of the progressive integration of the dopant, Cu, along with the increase in the reflux time interval of the nanosystems (Rasoul-al et al., 2013). The PL spectra of the MSA@Cu:ZnS nanosystems (Fig. 4b–f) and SC@Cu:ZnS nanosystems (Fig. 4h–l) are found to be broad and asymmetric, signifying the superposition of more than one peak. These PL spectra were deconvoluted using Gaussian curve fitting which resulted in their separation into three individual peaks for the synthesized nanosystems. The first band edge emission peak was found at a wavelength of ~400 nm and the second peak at ~450 nm, for both the nanosystems. The peaks at 400 nm and 450 nm may be due to the presence of native defect sites in the synthesized nanosystems (Jayanthi et al., 2007). The peak at ~500 nm is characteristic for copper based emission, which suggests the doping of the nanosystems by Cu (Bacherikov et al., 2014). Additionally, a shift in the band edge emissions from 390 to 410 nm and 450 to 470 nm in the nanosystems is observed with the increase in the period of synthesis. This may be due to the increase in the size of the particles, w.r.t the longer refluxing intervals (Rajesh et al., 2015).

3.2. Effect of pH on the size and the colloidal stability of the capped Cu:ZnS nanosystems

The variation in the hydrodynamic diameter of Cu:ZnS nanosystems as a function of their period of incubation at different solvent pH is shown in Fig. 5. From the figure it can be observed that the hydrodynamic diameter of the different variants does not show any significant change in relation to the incubation periods (up to 48 h).

Further, the size of the native Cu:ZnS nanoparticles, without any surface functionalization agent, was analysed as a function of their period of incubation with different solvent pH (Fig. S1). The hydrodynamic diameter of the native Cu:ZnS nanosystem was found to be significantly higher, compared to the MSA and SC functionalized nanosystems, across the solvent pH. This is indicative of a high degree of agglomeration in the native Cu:ZnS nanosystems, during the incubation process. Additionally, the smaller hydrodynamic diameter of the MSA and SC functionalized nanosystems is likely to impart a higher colloidal stability, compared to the native Cu:ZnS nanosystems.

The electrostatic stability of the capped Cu:ZnS nanosystems was also assessed as a function of the time period of incubation with different solvent pH, through the estimation of the correlated ζ potential (Fig. 6). The ζ potential of colloidal MSA@Cu:ZnS nanosystems was found to be in the range of (−29) to (−38) meV, while that of the SC@Cu:ZnS nanosystems was found to be (−26) to (−29) meV, over an extended time of incubation, across the pH range. Colloidal dispersions having a ζ potential $\geqslant \pm 30$ meV are generally considered to

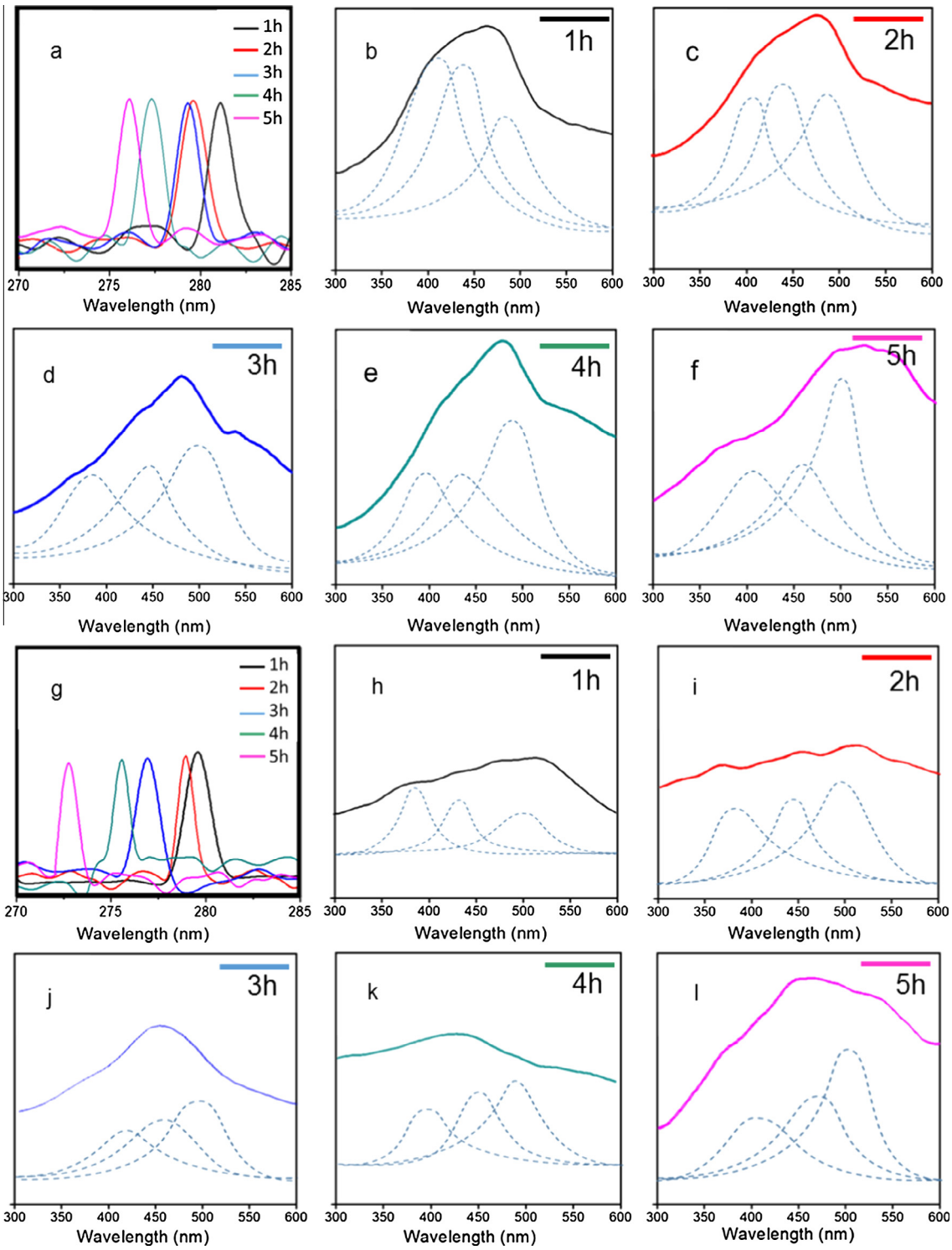

Figure 4 UV–vis absorption spectra of MSA@Cu:ZnS (a) and SC@Cu:ZnS (g) and PL spectra of MSA@Cu:ZnS (b–f) and SC@Cu:ZnS (h–l).

be highly stable, whereas dispersions having mean ζ potential values vicinal to zero are considered to be highly unstable, owing to their agglomeration (Mikolajczyk et al., 2015). The results suggest that aqueous suspensions of the MSA@Cu:ZnS nanosystems are likely to be highly stable in comparison with the SC@Cu:ZnS nanosystems, due to their relatively higher ζ potential. The ζ potential of the native Cu:ZnS nanosystems was also estimated and found to be < -20 meV (Fig. S1), that is strongly suggestive of its lower stability, compared to the MSA@Cu:ZnS and SC@Cu:ZnS nanosystems.

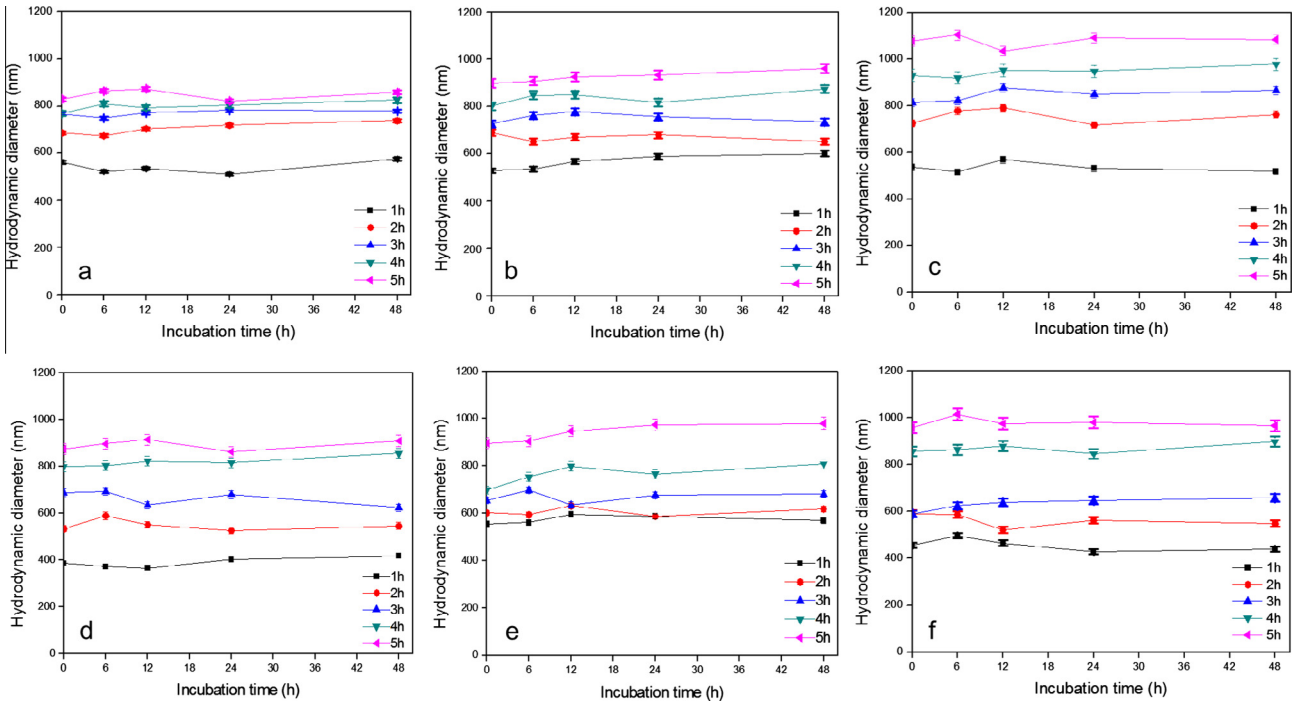

Figure 5 Hydrodynamic diameter of MSA@Cu:ZnS at pH 2 (a), 7 (b) and 12 (c) and SC@Cu:ZnS at pH 2 (d), 7 (e) and 12 (f).

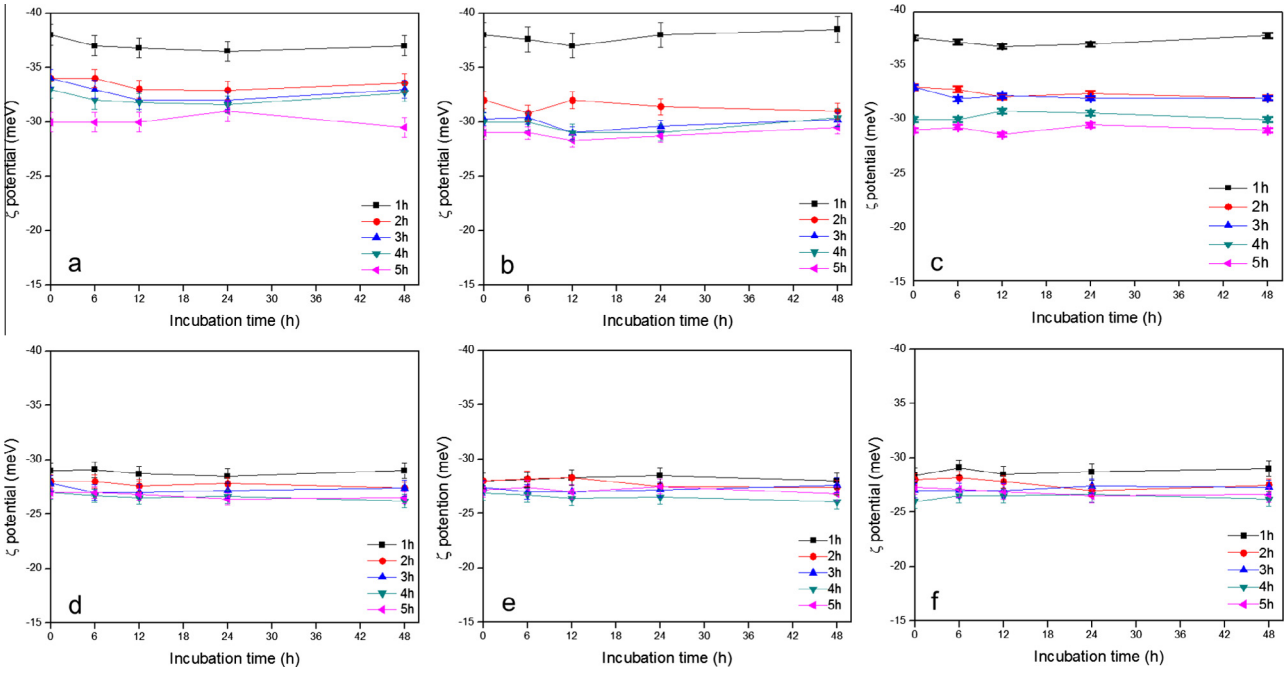

Figure 6 ζ potential of MSA@Cu:ZnS at pH 2 (a), 7 (b) and 12 (c) and SC@Cu:ZnS at pH 2 (d), 7 (e) and 12 (f).

3.3. Antibacterial assay

Fig. 7 shows the comparative analysis of the antibacterial efficacy of the two differentially capped Cu:ZnS nanosystems against Gram-negative *Escherichia coli* (NCTC 10538) and Gram-positive *Bacillus subtilis* (ATCC 11774) using disk diffusion assay. The 1 h variant of the MSA@Cu:ZnS nanosystems showed the largest area for the zone of inhibition, amongst all the variants, with an area of 1.29 cm^2 and 1.31 cm^2 against *E. coli* and *B. subtilis*, respectively, at a concentration of 5 mg ml^{-1}. The 1 h variant of the SC@Cu:ZnS nanosystems, showed the highest area for the zone of inhibition, amongst the SC capped time variants, with an area of 1.05 cm^2 and 1.18 cm^2 against *E. coli* and *B. subtilis* respectively at a concentration of 5 mg ml^{-1}. Further, the antibacterial activity of the native non-stabilized Cu:ZnS nanosystem was found to be

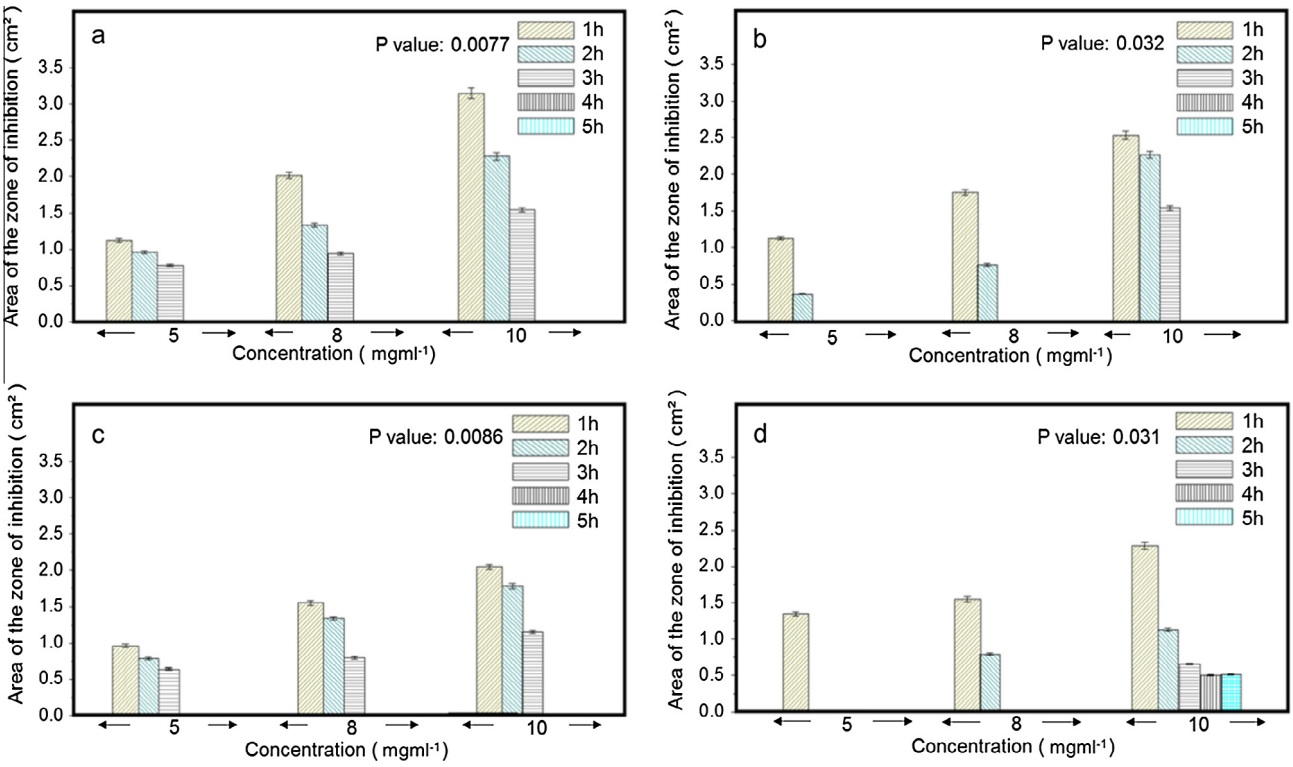

Figure 7 Comparison of the antibacterial properties of MSA@Cu:ZnS (a) and SC@Cu:ZnS (b) nanosystems against *E. coli* and MSA@Cu:ZnS (c) and SC@Cu:ZnS (d) against *B. subtilis*.

significantly lower than the MSA and SC functionalized nanosystems (Table S3).

In the context of the antibacterial studies with different concentration of the capped Cu:ZnS variants, a positive correlation between the area of zone of inhibition and the concentration of the nanoparticles used was observed (Table 1). Interestingly, a prominent zone of inhibition was seen at 5 mg ml^{-1} concentrations, for both the functionalized Cu:ZnS nanoparticles, which is significantly lower than the 10 mg ml^{-1} concentration, of the antibiotic standard (Ampicillin) used. The statistical significance of the disk diffusion assay was established through regression analysis and the

Table 1 Area of zone of inhibition for MSA @ Cu:ZnS and SC @ Cu:ZnS nanosystem against *E. coli* and *B. subtilis* for 1–5 h time variant.

Refluxed variants	Concentration of nanosystem (mg ml^{-1})	Area of zone of inhibition (cm^2)			
		MSA@Cu:ZnS		SC@Cu:ZnS	
		E. coli	*B. subtilis*	*E. coli*	*B. subtilis*
1 h	5	1.29 ± 0.02	1.31 ± 0.02	1.05 ± 0.02	1.18 ± 0.03
	8	1.96 ± 0.04	2.01 ± 0.03	1.54 ± 0.042	1.75 ± 0.03
	10	2.54 ± 0.05	3.14 ± 0.03	2.41 ± 0.069	2.27 ± 0.04
2 h	5	0.78 ± 0.02	0.94 ± 0.01	0.38 ± 0.07	–
	8	1.28 ± 0.02	1.33 ± 0.02	0.89 ± 0.01	0.78 ± 0.01
	10	1.96 ± 0.05	2.27 ± 0.03	2.27 ± 0.04	1.13 ± 0.02
3 h	5	0.50 ± 0.01	0.48 ± 0.01	–	–
	8	0.78 ± 0.02	0.97 ± 0.01	–	–
	10	1.31 ± 0.03	1.73 ± 0.01	1.54 ± 0.03	0.83 ± 0.01
4 h	5	–	–	–	–
	8	–	–	–	–
	10	–	–	–	0.60 ± 0.01
5 h	5	–	–	–	–
	8	–	–	–	–
	10	–	–	–	0.50 ± 0.01

obtained p value $\leqslant 0.05$ approves the relation between concentration of the variants used for antibacterial assay of nanoparticles and its antibacterial efficacy.

We have come across recent reports, which emphasize on the role of the size of the nanoparticles, as one of the important criteria influencing the antibacterial efficacy, when synthesized through solvothermal routes (Guzman et al., 2012; Agnihotri et al., 2014). In this context, we find that the 1 h refluxed variant of the MSA@Cu:ZnS nanosystems has the smallest size and also the highest antibacterial activity, that is in strong agreement with these reports. Further, the effects of refluxing leading to progressively larger nanoparticles, with more pronounced FTIR signatures of capping agents and the concomitant reduction in Zn crystallite signatures in the XRD diffractogram are seen in Fig. 3 (Singhal et al., 2012). These FTIR spectra, present a strong evidence in favor of intensive functionalization by the capping agents (Fig. 3), showing the progressive dominance of thiol (—SH) and carboxyl (—COOH) signatures, over the Cu and ZnS signatures, with the increase in refluxing intervals. The intensive capping results in the shielding of the antibacterial core thereby compromising the antibacterial efficacy of such functionalized nanosystems (Mohan et al., 2014). To eliminate the possibility of any free Cu^{2+} or Zn^{2+} contributing to the antibacterial activity of the initially refluxed samples, the concentration of Zn and Cu leachate from both the nanosystems, 48 h post incubation, was studied and is shown in Fig. S2. The concentration of Zn and Cu leachate for both the nanosystems is negligible compared to the total Zn and Cu present in the synthesized variants, with MSA@Cu:ZnS being more stable. We therefore infer that the antibacterial activity is primarily due to the as-prepared MSA@Cu:ZnS and SC@Cu:ZnS nanosystems.

The possible mechanism for the antibacterial action of the synthesized Cu:ZnS nanosystems may be proposed on the basis of existing reports that describe the antibacterial activity of native ZnS and Cu nanoparticles. ZnS nanoparticles have been reported to generate biologically reactive oxygen species including superoxide anions ($^{\cdot}O_2^-$), hydroxyl radicals ($^{\cdot}OH$) and hydroxyl ions (OH^-) which exert antibacterial activity by attacking cytoplasmic and extracytoplasmic targets (He et al., 2016). On the other hand, Cu^{2+} ions are known to strongly bind with the thiol (R—SH), imidazole ($C_3H_4N_2$), amino ($—NH_2$) and carboxyl (—COOH) groups of microbial membrane proteins, resulting in the increased cell permeability via aberrant regulation of transport through the membrane subsequently causing microbial cell death (Stanic et al., 2010). Furthermore, surfactants such as MSA have been reported to be highly effective as capping agents for the coating of antibacterial nanoparticles without significantly hindering their antibacterial activity (Taheri et al., 2014).

4. Conclusion

The present study showcases the synthesis of antibacterial Cu:ZnS nanosystems functionalized with Mercaptosuccinic acid and Sodium citrate through a solvothermal approach. The 1 h time variants of MSA@Cu:ZnS and SC@Cu:ZnS nanosystems were found to exhibit the most prominent zones of inhibition against both Gram-positive and Gram-negative bacteria. Further, the antibacterial activity of the 1 h MSA@Cu:ZnS variant was found to be the highest, along with a narrower size distribution and remarkable stability across the pH range. The study presents Cu:ZnS nanosystems as a novel class of antibacterial nanomaterials that show appreciable enhancement in antibacterial property when functionalized with MSA. Such materials are likely to find applications in the biomedical and food packaging industries as competent and cost effective antibacterial agents.

Acknowledgments

The authors wish to acknowledge DBT, Govt. of India, for the Research Grants (Grant No. BT/427/NE/TBP/2013 and BT/258/NE/TBP/2011), UGC, India for the Research Grants (TU/Fin/MBBT/116/05/11-12/64 and F.3-1/2015/DRS-II (SAP-II)) and DBT Strengthening Grant (BT/HRD/01/02/2007). They also thank Dr. Ratan Boruah, Tezpur University for the SEM and EDX analysis. They also sincerely thank Dr. S.K. Ray, Assoc. Prof., Dept. of Molecular Biology and Biotechnology for his inputs.

Appendix A. Supplementary material

Supplementary data associated with this article can be found, in the online version, at http://dx.doi.org/10.1016/j.arabjc.2016.05.002.

References

Agnihotri, S., Mukherji, S., Mukherji, S., 2014. Size-controlled silver nanoparticles synthesized over the range 5–100 nm using the same protocol and their antibacterial efficacy. RSC Adv. 4, 3974.

Agorku, E.S., Mamo, M.A., Mamba, B.B., Pandey, A.C., Mishra, A. K., 2015. Cobalt-doped ZnS-reduced graphene oxide nanocomposite as an advanced photocatalytic material. J. Porous Mater. 22, 47–56.

Bacherikov, Y.Y., Zelensky, S.E., Zhuk, A.G., Semenenko, N.A., Krylova, O.S., 2014. Luminescent properties of fine-dispersed ZnS:Cu prepared using self-propagating high-temperature synthesis. Semiconductor Phys., Quantum Electron. Optoelectron. 17, 374–379.

Bhuyan, T., Khanuja, M., Sharma, R., Patel, S., Reddy, M.R., Varma, S.A., 2015. A comparative study of pure and copper (Cu)-doped ZnO nanorods for antibacterial and photocatalytic applications with their mechanism of action. J. Nanopart. Res. 17, 288.

Bokare, A., Sanap, A., Pai, M., Sabharwal, S., Athawale, A.A., 2013. Antibacterial activities of Nd doped and Ag coated TiO_2 nanoparticles under solar light irradiation. Colloids Surf. B 102, 273–280.

Chauhan, R., Kumar, A., Chaudhary, R.P., 2014. Photocatalytic degradation of methylene blue with Cu doped ZnS nanoparticles. J. Lumin. 145, 6–12.

Cheng, C., Wen, Y., Xu, X., Gu, H., 2009. Tunable synthesis of carboxyl-functionalized magnetite nanocrystal clusters with uniform size. J. Mater. Chem. 19, 8782–8788.

Dhivya, C., Vandarkuzhali, S.A.A., Radha, N., 2015. Antimicrobial activities of nanostructured polyanilines doped with aromatic nitro compounds. Arab. J. Chem. http://dx.doi.org/10.1016/j.arabjc.2015.12.005.

Fang, X., Zhai, T., Gautam, U.K., Li, L., Wu, L., Bando, Y., Golberg, D., 2011. ZnS nanostructures: from synthesis to applications. Prog. Mater Sci. 56, 175–287.

Gao, F., Li, J., Wang, F., Yang, T., Zhao, D., 2015. Synthesis and characterization of high-quality water-soluble CdMnTe quantum dots capped by N-acetyl-L-cysteine through hydrothermal method. J. Lumin. 159, 32–37.

Guzman, M., Dille, J., Godet, S., 2012. Synthesis and antibacterial activity of silver nanoparticles against gram-positive and gram-negative bacteria. Nanomed. Nanotechnol. Biol. Med. 8, 37–45.

He, w., Jia, H., Cai, J., Han, X., Zheng, Z., Wamer, W.G., Yin, J., 2016. Production of reactive oxygen species and electrons from photoexcited ZnO and ZnS nanoparticles: a comparative study for unraveling their distinct photocatalytic activities. J. Phys. Chem. C. http://dx.doi.org/10.1021/acs.jpcc.5b11456.

Jayanthi, k., Chawla, S., Chander, H., Haranath, D., 2007. Structural, optical and photoluminescence properties of ZnS: Cu nanoparticle thin films as a function of dopant concentration and quantum confinement effect. Cryst. Res. Technol. 42, 976–982.

Kuppayee, M., Nachiyar, G.K.V., Ramasamy, V., 2011. Synthesis and characterization of Cu^{2+} doped ZnS nanoparticles using TOPO and SHMP as capping agents. Appl. Surf. Sci. 257, 6779–6786.

Lee, G., Anandan, S., Masten, S.J., Wu, J.J., 2014. Sonochemical synthesis of hollow copper doped zinc sulfide nanostructures: optical and catalytic properties for visible light assisted photosplitting of water. Ind. Eng. Chem. Res. 53, 8766–8772.

Mikolajczyk, A., Gajewicz, A., Rasulev, B., Schaeublin, N., Maurer-Gardner, E., Hussain, S., Leszczynski, J., Puzyn, T., 2015. Zeta potential for metal oxide nanoparticles: a predictive model developed by a nano-quantitative structure–property relationship approach. Chem. Mater. 27, 2400–2407.

Mohan, S., Oluwafemi, S.O., George, S.C., Jayachandran, V.P., Lewu, F.B., Songca, S.P., Kalarikkal, N., Thomas, S., 2014. Completely green synthesis of dextrose reduced silver nanoparticles, its antimicrobial and sensing properties. Carbohydr. Polym. 106, 469–474.

Murugadoss, G., 2012. Luminescence properties of co-doped ZnS:Ni, Mn and ZnS:Cu, Cd nanoparticles. J. Lumin. 132, 2043–2048.

Namsani, S., Nair, N.N., Singh, J.K., 2015. Interaction potential models for bulk ZnS, ZnS nanoparticle, and ZnS nanoparticle-PMMA from first-principles. J. Comput. Chem. 36, 1176–1186.

Pelgrift, R.Y., Friedman, A.J., 2013. Nanotechnology as a therapeutic tool to combat microbial resistance. Adv. Drug Deliv. Rev. 65, 1803–1815.

Rajesh, C., Phadnis, C.V., Sonawane, K.G., Mahamuni, S., 2015. Synthesis and optical properties of copper-doped ZnSe quantum dots. Phys. Scr. 90, 015803 (8pp).

Rasoul- al, K.T., Abbas, N.K., Shanan, Z.J., 2013. Structural and optical characterization of Cu and Ni doped ZnS nanoparticles. Int. J. Electrochem. Sci. 8, 5594–5604.

Reghuram, S., Arivarasan, A., Kalpana, R., Jayavel, R., 2015. CdSe and CdSe/ZnS quantum dots for the detection of C-reactive protein. J. Exp. Nanosci. 10, 787–802.

Ruparelia, J.P., Chatterjee, A.K., Duttagupta, S.P., Mukherji, S., 2008. Strain specificity in antimicrobial activity of silver and copper nanoparticles. Acta Biomater. 4, 707–716.

Singh, P., Sharma, P.K., Kumar, M., Dutta, R., Sundaram, S., Pandey, A.C., 2014. Red luminescent manganese-doped zinc sulphide nanocrystals and their antibacterial study. J. Mater. Chem. B 2, 522–528.

Singhal, S., Kaur, J., Namgyal, T., Sharma, R., 2012. Cu-doped ZnO nanoparticles: synthesis, structural and electrical properties. Physica B 407, 1223–1226.

Stanic, V., Dimitrijevĭc, S., Stankovĭc, J.A., Mitrĭc, M., Jokĭ, B., Plé cas, I.B., Raĭcevi, S., 2010. Synthesis, characterization and antimicrobial activity of copper and zinc-doped hydroxyapatite nanopowders. Appl. Surf. Sci. 256, 6083–6089.

Suyana, P., Kumar, S.N., Kumar, B.S.D., Nair, B.N., Pillai, S.C.A., Mohamed, P., Warrier, K.G.K., Hareesh, U.S., 2014. Antifungal properties of nanosized ZnS particles synthesized by sonochemical precipitation. RSC Adv. 4, 8439–8445.

Talebian, N., Amininezhad, S.M., Doudi, M., 2013. Controllable synthesis of ZnO nanoparticles and their morphology-dependent antibacterial and optical properties. J. Photochem. Photobiol., B 120, 66–73.

Taheri, S., Cavallaro, A., Christo, S.N., Smith, L.E., Majewski, P., Barton, M., Hayball, J.D., Vasilev, K., 2014. Substrate independent silver nanoparticle based antibacterial coatings. Biomaterials 35, 4601–4609.

Tam, K.H., Djurišić, A.B., Chan, C.M.N., Xi, Y.Y., Tse, C.W., Leung, Y.H., Chan, W.K., Leung, F.C.C., Au, D.W.T., 2008. Antibacterial activity of ZnO nanorods prepared by a hydrothermal method. Thin Solid Films 516, 6167–6174.

Wu, C., Shen, L., Yu, H., Zhang, Y., Huang, Q., 2012. Solvothermal synthesis of Cu-doped ZnO nanowires with visible light-driven photocatalytic activity. Mater. Lett. 74, 236–238.